2013 IEEE/RSJ International Conference on
Intelligent Robots and Systems (IROS)
November 3-7, 2013. Tokyo, Japan

Uncalibrated Visual Servoing of Nonholonomic Mobile Robots

Baoquan Li, Yongchun Fang, *Senior Member, IEEE*, and Xuebo Zhang, *Member, IEEE*

***Abstract*—In this paper, an uncalibrated visual servo regulation strategy is designed for a nonholonomic mobile robot equipped with an eye-in-hand camera, which drives the mobile robot to the target pose with exponential convergence. Specifically, a novel fundamental matrix-based algorithm is firstly proposed to rotate the robot to point toward the desired position, with the camera intrinsic parameters estimated simultaneously by employing the fundamental matrix and a projection homography matrix. Subsequently, by utilizing the obtained camera intrinsic parameters, a straight-line motion controller is developed to drive the robot to the desired position, with the orientation of the robot always facing the target position. Another pure rotation controller is finally adopted to correct the orientation error. The exponentially convergent properties of the visual servo errors are proven with mathematical analysis. The performance of the proposed uncalibrated visual servo regulation method is further validated by simulation results.**

I. Introduction

The flexibility, intelligence and precision of mobile robots can be greatly increased after introducing vision sensors. The control of mobile robots by using visual information has been widely studied in recent years [1]-[5]. This technique, termed as visual servoing of mobile robots, can be used in lots of applications, such as intelligent transportation, family services, and so on. However, most of the existing methods generally construct the visual servoing controller by utilizing the intrinsic parameters of the cameras. In this sense, cameras must be carefully calibrated beforehand, and the controllers are usually over-sensitive to camera calibration errors. This drawback limits the further applications of mobile robots controlled by image feedback. Therefore, a new method is highly demanded for visual servoing of mobile robots by using an uncalibrated camera. Moreover, unlike traditional six degree-of-freedom robot manipulators visual servoing research [6]-[8], mobile robots are subject to nonholonomic constraints, which brings even more challenges for visual servo regulation tasks [9]. Besides, the lacks of 3-D model of the scene and depth information are inherent problems for monocular vision systems [10]. As a consequence, these challenges make the task of uncalibrated visual servo regulation for mobile robots even more difficult.

To accomplish the visual servoing tasks with an uncalibrated or imperfect calibrated camera, various methods for robot manipulators have been developed so far [11]-[15]. Malis *et al.* analyze the robustness of the 2.5-D visual servoing scheme with respect to camera calibration errors, and provide the relevant conditions for convergent property under calibration errors [11]. To cope with imperfect calibration of the camera, Hu *et al.* design a high-gain robust controller to stabilize the rotation error, and an adaptive controller to stabilize the translation errors while compensating for the uncertainties of unknown depth information and camera intrinsic parameters [12]. In [13], Liu *et al.* design a depth-independent interaction matrix to make camera intrinsic parameters appear linearly in the closed-loop dynamics, then adaptive algorithms and Lyapunov techniques are used to develop a controller to regulate the image errors with an uncalibrated camera. However, these strategies are developed only for six degrees of freedom robot manipulators, and it is extremely difficult to extend them for mobile robots because of the nonholonomic motion constraint.

For the visual servoing problem of a nonholonomic mobile robot utilizing an eye-to-hand uncalibrated camera, many solutions have been developed, such as the results given in [16] and [17]. Most of these results address the mobile robot tracking control problem. For example, to fulfill the global asymptotic tracking control task of a nonholonomic mobile robot with an uncalibrated camera, Dixon *et al.* develop an adaptive tracking controller in [16] to compensate for uncertain camera and mechanical parameters. It should be pointed out that, due to the existence of the nonholonomic constraint, regulation tasks for a mobile robot are far more difficult than tracking ones [9]. For this problem, Wang *et al.* use an imperfect calibrated camera to regulate a mobile robot to the desired pose. To accomplish the uncalibrated visual servo task, they design a robust controller by using dynamic feedback and two-step techniques [17]. Unfortunately, the available methods are usually designed under the eye-to-hand vision frame, whose application potentials are badly limited since the mobile robot needs to be within a small area to enable the camera to capture its image. On the other hand, for the eye-in-hand configuration, the camera intrinsic parameters enter into the closed-loop dynamics through a nonlinear manner, which makes it extremely difficult to design a controller to address the camera parameters uncertainty. So far, it is still a very challenging and interesting problem in the visual servoing field to accomplish the regulation task for a nonholonomic mobile robot by employing an uncalibrated eye-in-hand camera.

In this paper, an efficient visual servo regulation strategy is designed for a nonholonomic mobile robot by utilizing an

This work is supported in part by Specialized Research Fund for the Doctoral Program of Higher Education of China under Grant 20120031120040, in part by National Natural Science Foundation of China under Grant 61203333, and in part by Tianjin Natural Science Foundation under Grant 13JCQNJC03200.

B. Li, Y. Fang, and X. Zhang are with the Institute of Robotics and Automatic Information Systems (IRAIS), Tianjin Key Laboratory of Intelligent Robotics, Nankai University, Tianjin, 300071, P. R. China, email: yfang@robot.nankai.edu.cn.

uncalibrated eye-in-hand camera, with which, not only is the visual servo regulation task accomplished, but also the camera intrinsic parameters are estimated simultaneously. The proposed visual servoing regulation scheme consists of three stages, where the first stage rotates the mobile robot to point to the desired position, with the camera intrinsic parameters obtained simultaneously, and the second stage designs a straight-line motion controller to drive the robot to the desired position, while the third stage compensates the orientation error by a pure rotation control law. The proposed visual servo regulation scheme achieves exponentially convergent properties, which are proven with rigorous mathematical analysis. Simulation results are collected to validate the effectiveness of the uncalibrated visual servoing strategy. The main contribution of this paper includes the following aspects: 1) the uncalibrated eye-in-hand visual servo regulation problem is successfully solved; 2) exponential stability and straight line servoing path are achieved, which convincingly indicates high servo efficiency; 3) intrinsic parameters of the camera are obtained to facilitate other subsequent tasks.

I. Problem Formulation

A. System Description

As illustrated in Fig. 1, the coordinate system of the onboard camera is supposed to be coincident with the nonholonomic mobile robot. Let the orthogonal coordinate system $\mathcal{F}^*$ denote the desired pose of the camera, and the origin of $\mathcal{F}^*$ (optical center of camera) locate at the midpoint of the wheels axis. The z_c^* axis of $\mathcal{F}^*$ is along the camera optical axis, which is supposed to be aligned with the front of the robot, the x_c^* axis is parallel to the wheel axis, and the y_c^* axis is orthogonal to the $z_c^* x_c^*$ plane (the motion plane of the robot). Additionally, we define frame $\mathcal{F}^c$ to represent the current pose of the camera. The angle $\theta(t)$ represents the rotation angle of $\mathcal{F}^c$ w.r.t. $\mathcal{F}^*$.

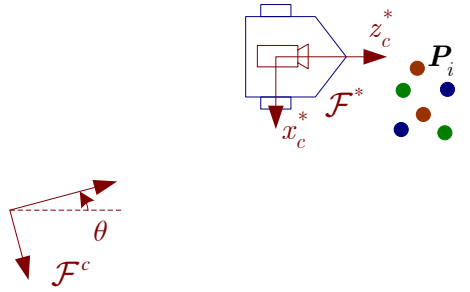

Fig. 1. Coordinate systems relationship of the visual servoing task.

There exist N static feature points $\boldsymbol{P}_i (i = 1,2,...,N)$ in the scene, and the images taken at $\mathcal{F}^*$ and $\mathcal{F}^c$ are denoted as the desired and current images, respectively. The visual servo regulation task aims to drive the robot so as to make $\mathcal{F}^c$ coincide with $\mathcal{F}^*$ by using image feedback. Furthermore, it is assumed that the feature points remain in the field of camera view during the visual servoing process.

B. Control Scheme

The objective of this paper is to construct a proper visual servo controller to regulate the pose of a nonholonomic mobile robot by utilizing image information obtained from an uncalibrated eye-in-hand camera. The block diagram of the proposed strategy is shown in Fig. 2. During the servo process, the desired and current images are used to estimate a fundamental matrix and a projection homography matrix. In stage 1, the fundamental matrix is utilized to make the robot point to the target position, while the projection homography matrix is employed to estimate the camera intrinsic parameters. In stage 2, the robot is controlled to move in a straight line to reach the target position, and it rotates to the desired orientation by utilizing the control law proposed in stage 3. As a sequence, highly efficient straight-line visual servoing path is obtained, even with unknown camera intrinsic parameters.

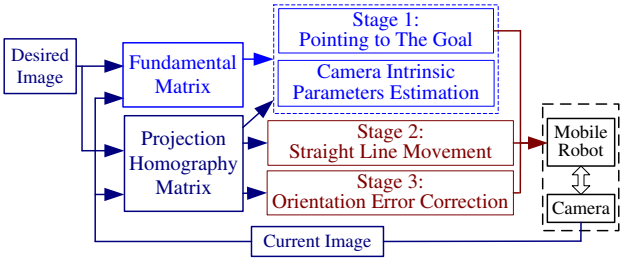

Fig. 2. Block diagram of the proposed strategy.

C. Coordinate Systems Relationship

Without loss of generality, we take $\mathcal{F}^*$ as the reference coordinate system, while the rotation matrix and the translation vector of $\mathcal{F}^c$ w.r.t. $\mathcal{F}^*$ are denoted as ${}^*_c\boldsymbol{R}$ and ${}^*\boldsymbol{t}_c$, respectively. By taking into account the planar motion constraint of the robot, ${}^*_c\boldsymbol{R}$ and ${}^*\boldsymbol{t}_c$ have the following form:

$$ {}^*_c\boldsymbol{R} = \begin{bmatrix} c\theta & 0 & -s\theta \\ 0 & 1 & 0 \\ s\theta & 0 & c\theta \end{bmatrix}, \quad {}^*\boldsymbol{t}_c = \begin{bmatrix} {}^*t_{cx} \\ 0 \\ {}^*t_{cz} \end{bmatrix} \tag{1} $$

where $s\theta \triangleq \sin\theta$, $c\theta \triangleq \cos\theta$, ${}^*t_{cx}$ and ${}^*t_{cz}$ represent the x and z coordinates of the origin of $\mathcal{F}^c$ expressed in $\mathcal{F}^*$, respectively. Thus, the current pose of the robot in $\mathcal{F}^*$ can be expressed as $({}^*t_{cz}, {}^*t_{cx}, \theta)$, and the regulation task is accomplished when $({}^*t_{cz}, {}^*t_{cx}, \theta) = (0,0,0)$.

Similarly, the rotation matrix and the translation vector of $\mathcal{F}^*$ w.r.t. $\mathcal{F}^c$ are denoted as ${}^c_*\boldsymbol{R}$ and ${}^c\boldsymbol{t}_*$:

$$ {}^c_*\boldsymbol{R} = \begin{bmatrix} c\theta & 0 & s\theta \\ 0 & 1 & 0 \\ -s\theta & 0 & c\theta \end{bmatrix}, \quad {}^c\boldsymbol{t}_* = \begin{bmatrix} {}^ct_{*_x} \\ 0 \\ {}^ct_{*_z} \end{bmatrix}, \tag{2} $$

where ${}^ct_{*_x}$ and ${}^ct_{*_z}$ represent the x and z coordinates of the origin of $\mathcal{F}^*$ expressed in $\mathcal{F}^c$, respectively.

D. System Kinematics

According to the kinematic model of the robot, we know:

$$ {}^*\dot{t}_{cz} = v_c c\theta, \quad {}^*\dot{t}_{cx} = -v_c s\theta, \quad \dot{\theta} = w_c \tag{3} $$

where v_c and w_c represent the linear and angular velocities of the camera/robot. From coordinate transformation rules, it can be known that

$$ {}^{c}\boldsymbol{t}_{*} = -{}^{c}_{*}\boldsymbol{R}\,{}^{*}\boldsymbol{t}_{c} \,. \tag{4} $$

After expanding (4), the following formula can be obtained

$$ \begin{cases} {}^{c}t_{*_x} = -{}^{*}t_{cx}c\theta - {}^{*}t_{cz}s\theta \\ {}^{c}t_{*_z} = +{}^{*}t_{cx}s\theta - {}^{*}t_{cz}c\theta. \end{cases} \tag{5} $$

After taking the time derivative of (5) and substituting (3) into the resulting expression, we obtain

$$ \begin{cases} {}^{c}\dot{t}_{*_x} = {}^{c}t_{*_z}w_c \\ {}^{c}\dot{t}_{*_z} = -v_c - {}^{c}t_{*_x}w_c \\ \dot{\theta} = w_c. \end{cases} \tag{6} $$

II. Stage 1: Pointing To The Target Position

In this section, the robot is driven toward the target position, and the camera intrinsic parameters are also estimated.

A. Configuration of Target Position Pointing

The essential matrix relating $\mathcal{F}^*$ and $\mathcal{F}^c$ is denoted as $\boldsymbol{E}^{*c}$, which is defined by [18]:

$$ \boldsymbol{E}^{*c} \triangleq [{}^{*}\boldsymbol{t}_c]_{\times}\,{}^{*}\boldsymbol{R} \,. \tag{7} $$

A fundamental matrix denoted as $\boldsymbol{F}^{*c}$ has the following relationship with $\boldsymbol{E}^{*c}$:

$$ \boldsymbol{F}^{*c} = \boldsymbol{K}^{-T}\boldsymbol{E}^{*c}\boldsymbol{K}^{-1} \tag{8} $$

where $\boldsymbol{K}$ represents the camera intrinsic parameters matrix:

$$ \boldsymbol{K} = \begin{bmatrix} f_u & 0 & u_0 \\ 0 & f_v & v_0 \\ 0 & 0 & 1 \end{bmatrix} \tag{9} $$

with (u_0, v_0) denoting the image principle point, f_u, f_v being the focal length expressed in pixels at the directions of $\mathbf{u}$- and $\mathbf{v}$- axes, respectively.

After substituting (9), (1) and (7) into (8), the form of $\boldsymbol{F}^{*c}$ can be obtained as:

$$ \boldsymbol{F}^{*c} = \begin{bmatrix} 0 & -\dfrac{{}^{*}t_{cz}}{f_u f_v} & \dfrac{v_0\,{}^{*}t_{cz}}{f_u f_v} \\ \dfrac{{}^{*}t_{cz}c\theta - {}^{*}t_{cx}s\theta}{f_u f_v} & 0 & F^{*c}_{23} \\ -\dfrac{v_0({}^{*}t_{cz}c\theta - {}^{*}t_{cx}s\theta)}{f_u f_v} & \dfrac{u_0\,{}^{*}t_{cz}}{f_u f_v} + \dfrac{{}^{*}t_{cx}}{f_v} & F^{*c}_{33} \end{bmatrix} \tag{10} $$

where F^{*c}_{23} and F^{*c}_{33} represent relevant entities of $\boldsymbol{F}^{*c}$, and F^{*c}_{23} has the following form:

$$ F^{*c}_{23} = -\frac{u_0({}^{*}t_{cz}c\theta - {}^{*}t_{cx}s\theta)}{f_u f_v} + \frac{-{}^{*}t_{cz}s\theta - {}^{*}t_{cx}c\theta}{f_v}. \tag{11} $$

After normalizing $\boldsymbol{F}^{*c}$ by F^{*c}_{12} in the premise of ${}^{*}t_{cz} \neq 0$, and then utilizing (5), the resulting matrix, which is denoted as $\boldsymbol{F}^{*c}_{S}$, can be obtained as follows:

$$ \boldsymbol{F}^{*c}_{S} = \begin{bmatrix} 0 & 1 & -v_0 \\ \dfrac{{}^{c}t_{*_z}}{{}^{*}t_{cz}} & 0 & \dfrac{u_0\,{}^{c}t_{*_z} + f_u\,{}^{c}t_{*_x}}{-{}^{*}t_{cz}} \\ \dfrac{-v_0\,{}^{c}t_{*_z}}{{}^{*}t_{cz}} & \dfrac{u_0\,{}^{*}t_{cz} + f_u\,{}^{*}t_{cx}}{-{}^{*}t_{cz}} & F_{S33} \end{bmatrix}. \tag{12} $$

The i th desired image point and its corresponding current image point are denoted by $\boldsymbol{p}^*_i$ and $\boldsymbol{p}^c_i$, respectively, which are explicitly expressed as

$$ \boldsymbol{p}^*_i = \begin{bmatrix} u^*_i & v^*_i & 1 \end{bmatrix}^T, \quad \boldsymbol{p}^c_i = \begin{bmatrix} u^c_i & v^c_i & 1 \end{bmatrix}^T. \tag{13} $$

At least six pairs of matched feature points are needed to estimate $\boldsymbol{F}^{*c}$ up to scale by the following relationship [18]:

$$ (\boldsymbol{p}^*_i)^T \boldsymbol{F}^{*c}\boldsymbol{p}^c_i = 0 \tag{14} $$

where $\boldsymbol{F}^{*c}_{S}$ is obtained after normalizing F^{*c}_{12}.

After estimating $\boldsymbol{F}^{*c}_{S}$, one of the camera intrinsic parameters v_0 can be obtained from (12) as:

$$ v_0 = -F^{*c}_{S13} \tag{15} $$

where F^{*c}_{Sij} denotes the element locating at i th row, j th column of $\boldsymbol{F}^{*c}_{S}$.

Fig. 3 shows the coordinate systems when the robot locates at its initial pose, and without loss of generality, the initial pose of the robot is assumed behind the desired pose. When the robot implements pure rotation, ${}^{*}t_{cz}$ keeps constant, and ${}^{c}t_{*_z}$ becomes largest when the robot faces toward the target position. Thus, it can be known that when the measurable signal F^{*c}_{S21} in (12) reaches its minimum value, the robot points toward the desired position.

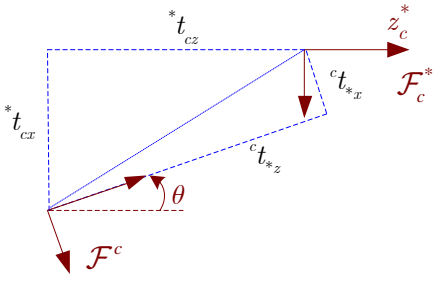

Fig. 3. Coordinate systems when the robot locates at its initial pose.

Based on the previous analysis, a constant w_c can be set for the robot to make F^{*c}_{S21} reaches its minimum $F^{*c}_{S21\min}$, which implies the fact of ${}^{*}t_{cx}=0$. We denote the value of F^{*c}_{S21} and F^{*c}_{S23} at this moment as $F^{*c}_{S21\text{spe}}$ and $F^{*c}_{S23\text{spe}}$, respectively, then based on the expression of (12), u_0 can be obtained as:

$$u_0 = -\frac{F^{*c}_{S23\text{spe}}}{F^{*c}_{S21\text{spe}}}. \tag{16}$$

Remark 1: If the robot is initially at the special location so that ${}^{*}t_{cz}$ equals to zero, singularity problem occurs when normalizing $\boldsymbol{F}^{*c}$ by F^{*c}_{12}. This special situation can be detected without much difficulty in the process of $\boldsymbol{F}^{*c}$ estimation. In this case, one solution is to drive the robot to make a back motion first of all so as to make ${}^{*}t_{cz}\neq 0$.

B. Rotation Controller Design and Analysis

After obtaining $F^{*c}_{S21\min}$, we can rotate the robot toward the target position with the robot linear velocity set as $v_c=0$. Based on the previous analysis, the error signal for Stage 1 is defined as

$$e_1 \triangleq F^{*c}_{S21} - F^{*c}_{S21\min}. \tag{17}$$

Obviously, the robot faces toward the target position when $e_1(t)$ is regulated to zero. Taking the time derivative of (17) yields:

$$\dot{e}_1 = \dot{F}^{*c}_{S21}. \tag{18}$$

After utilizing (12) and (6), we can transform (18) into

$$\dot{e}_1 = -\frac{1}{{}^{*}t_{cz}}\,{}^{c}t_{*x}\,w_c. \tag{19}$$

From (12), it can be shown that

$$\frac{{}^{c}t_{*x}}{{}^{*}t_{cz}} = -\frac{u_0F^{*c}_{S21}+F^{*c}_{S23}}{f_u}. \tag{20}$$

After substituting (20) into (19), the open-loop error system turns into

$$\dot{e}_1 = \frac{u_0F^{*c}_{S21}+F^{*c}_{S23}}{f_u}\,w_c. \tag{21}$$

To meet the control objective, the following rotation controller is designed:

$$v_c=0,\ w_c=-k_1\left(\left(-\frac{F^{*c}_{S23\text{spe}}}{F^{*c}_{S21\text{spe}}}\right)F^{*c}_{S21}+F^{*c}_{S23}\right)e_1 \tag{22}$$

where $k_1\in\mathbb{R}^{+}$ is a control gain.

Theorem 1: The controller (22) regulates the error signal $e_1(t)$ defined in (17) to zero exponentially fast.

Proof: Details are available upon request.

C. Estimation of Camera Parameter f_u

We have obtained u_0 and v_0 in part A, f_u will be estimated in this part. Firstly, the following translational transform is implemented to move the principle point to $(0,0)$:

$$\begin{cases} u_i^{*\prime}=u_i^{*}-u_0 \\ v_i^{*\prime}=v_i^{*}-v_0 \end{cases},\quad \begin{cases} u_i^{c\prime}=u_i^{c}-u_0 \\ v_i^{c\prime}=v_i^{c}-v_0 \end{cases}. \tag{23}$$

Then the camera intrinsic parameters (9) becomes

$$\boldsymbol{K}_{(u_0,v_0=0)}=\begin{bmatrix} f_u & 0 & 0\\ 0 & f_v & 0\\ 0 & 0 & 1\end{bmatrix}. \tag{24}$$

Meanwhile, we denote $\boldsymbol{p}_i^{*\prime}$ and $\boldsymbol{p}_i^{c\prime}$ as the desired and current image points w.r.t. the transformed principle point $(0,0)$, respectively:

$$\boldsymbol{p}_i^{*\prime}\triangleq\begin{bmatrix}u_i^{*\prime} & v_i^{*\prime} & 1\end{bmatrix}^T,\quad \boldsymbol{p}_i^{c\prime}\triangleq\begin{bmatrix}u_i^{c\prime} & v_i^{c\prime} & 1\end{bmatrix}^T. \tag{25}$$

We denote $\boldsymbol{G}$ as a projection homography matrix [3]:

$$\boldsymbol{G}\triangleq\boldsymbol{K}_{(u_0,v_0=0)}\left({}^{c}_{*}\boldsymbol{R}+\frac{{}^{c}\boldsymbol{t}_{*}}{d^{*}}(\boldsymbol{n}^{*})^T\right)\boldsymbol{K}^{-1}_{(u_0,v_0=0)} \tag{26}$$

where $\boldsymbol{n}^{*}\triangleq[n^{*}_x,n^{*}_y,n^{*}_z]^T$ is a unit vector normal to the relevant feature points plane expressed in $\mathcal{F}^{*}$, and $d^{*}\in\mathbb{R}$ is the unknown distance from the origin of $\mathcal{F}^{*}$ to the feature points plane along $\boldsymbol{n}^{*}$. After expanding (26), we obtain

$$\boldsymbol{G}=\begin{bmatrix} c\theta+\dfrac{{}^{c}t_{*x}n^{*}_x}{d^{*}} & \dfrac{f_u}{f_v}\dfrac{{}^{c}t_{*x}n^{*}_y}{d^{*}} & f_u\left(s\theta+\dfrac{{}^{c}t_{*x}n^{*}_z}{d^{*}}\right)\\ 0 & 1 & 0\\ \dfrac{1}{f_u}\left(-s\theta+\dfrac{{}^{c}t_{*z}n^{*}_x}{d^{*}}\right) & \dfrac{1}{f_v}\dfrac{{}^{c}t_{*z}n^{*}_y}{d^{*}} & c\theta+\dfrac{{}^{c}t_{*z}n^{*}_z}{d^{*}}\end{bmatrix}. \tag{27}$$

The matrix $\boldsymbol{G}$ can be estimated by using $\boldsymbol{p}_i^{*\prime}$ and $\boldsymbol{p}_i^{c\prime}$ through the following relationship:

$$\boldsymbol{p}_i^{c\prime}=\lambda_i\boldsymbol{G}\boldsymbol{p}_i^{*\prime} \tag{28}$$

where λ_i is a coefficient. It can be known from (28) that three corresponding feature points are enough to estimate $\boldsymbol{G}$.

Particularly, the form of $\boldsymbol{G}$ can be simplified when ${}^{c}t_{*x}=0$, with the result denoted as $\boldsymbol{G}({}^{c}t_{*x}=0)$:

$$\boldsymbol{G}({}^{c}t_{*x}=0)=\begin{bmatrix} c\theta & 0 & f_us\theta\\ 0 & 1 & 0\\ \dfrac{1}{f_u}\left(-s\theta+\dfrac{{}^{c}t_{*z}n^{*}_x}{d^{*}}\right) & \dfrac{1}{f_v}\dfrac{{}^{c}t_{*z}n^{*}_y}{d^{*}} & c\theta+\dfrac{{}^{c}t_{*z}n^{*}_z}{d^{*}}\end{bmatrix}. \tag{29}$$

We denote $\boldsymbol{G}({}^{c}t_{*_x}=0)$ and $\theta(t)$ at the end of Stage 1 as $\boldsymbol{G}_{\text{spe}}$ and θ_{spe}, respectively. The symbol $G_{\text{spe}ij}$ denotes the element locating at i th row, j th column of $\boldsymbol{G}_{\text{spe}}$.

When the robot points to the desired position, it is known that $\theta \in (-\pi/2, \pi/2)$, we can then obtain θ_{spe} as follows:

$$\theta_{\text{spe}} = \begin{cases} \arccos G_{\text{spe11}}, \text{ if } G_{\text{spe13}} > 0 \\ -\arccos G_{\text{spe11}}, \text{ if } G_{\text{spe13}} < 0 \end{cases}. \tag{30}$$

From (29) and (30), f_u can be obtained as:

$$f_u = \frac{G_{\text{spe13}}}{\sin\theta_{\text{spe}}}. \tag{31}$$

Remark 2: For the relationship (31), singularity will appear when $\sin\theta_{\text{spe}} = 0$, which corresponds to the special situation that the initial value of ${}^{*}t_{cx}$ is zero. In this situation, the robot will be aligned with the desired pose after stage 1, then a linear velocity controller can be used to accomplish the visual regulation task [19].

Remark 3: Based on the fact that for a common camera, f_v is usually close to f_u, the same estimation for f_u can be also given to f_v. In this sense, the four intrinsic camera parameters have been estimated in this stage.

III. Stage 2: Straight Line Movement

When the robot points to the desired position, a straight-line motion controller is developed in Stage 2. Due to the image noise and external disturbances in real situations, the orientation of the robot may slightly deviate from the direction pointing to the goal, leading $\boldsymbol{G}({}^{c}t_{*_x}=0)$ degenerates to $\boldsymbol{G}$. Thus we need to design w_c to adjust the orientation of the robot in this stage as well.

In this stage, the system errors are defined by utilizing the entities of $\boldsymbol{G}$:

$$e_{2v} \triangleq \frac{G_{\text{spe13}}}{\sin\theta_{\text{spe}}} G_{32}, \quad e_{2w} \triangleq G_{12}, \tag{32}$$

where the signal e_{2w} is introduced to design w_c, so as to keep the robot always pointing to the goal in stage 2. As far as the feature points plane, which has been used to estimate $\boldsymbol{G}$ previously, is not vertical to the robot motion plane, the normal vector $n_y^* \neq 0$, then from (35), it can be seen that if the error signals e_{2v}, e_{2w} are regulated to zero, the robot reaches the desired position.

Taking the time derivative of (32) yields:

$$\dot{e}_{2v} = f_u \frac{1}{f_v} \frac{{}^{c}\dot{t}_{*_z} n_y^*}{d^*}, \quad \dot{e}_{2w} = \frac{f_u}{f_v} \frac{{}^{c}\dot{t}_{*_x} n_y^*}{d^*}. \tag{33}$$

After substituting (6) into (33) and utilizing the expressions of (32), the following dynamics can be obtained:

$$\begin{bmatrix} \dot{e}_{2v} \\ \dot{e}_{2w} \end{bmatrix} = \begin{bmatrix} -\xi & -e_{2w} \\ 0 & e_{2v} \end{bmatrix} \begin{bmatrix} v_c \\ w_c \end{bmatrix} \tag{34}$$

where ξ denotes an unknown constant

$$\xi \triangleq f_u \frac{1}{f_v} \frac{n_y^*}{d^*}. \tag{35}$$

For the error system (37), the following feedback linearization controller is designed:

$$\begin{bmatrix} v_c \\ w_c \end{bmatrix} = \begin{bmatrix} \dfrac{1}{-\widehat{\xi}} & \dfrac{e_{2w}}{-\widehat{\xi} e_{2v}} \\ 0 & \dfrac{1}{e_{2v}} \end{bmatrix} \begin{bmatrix} -k_{2v} e_{2v} \\ -k_{2w} e_{2w}^{\kappa/\eta} \end{bmatrix} \tag{36}$$

where $k_{2v}, k_{2w} \in \mathbb{R}^+$ are control gains, κ, η are positive odd integers with $\kappa < \eta$, and $\widehat{\xi}$ is the best-guess estimation for ξ with the requirement of

$$\text{sgn}(\widehat{\xi}) = \text{sgn}(\xi). \tag{37}$$

It is worthwhile to point out that the sign of ξ is equal to that of n_y^*, which can be easily determined from G_{32}.

Theorem 2: The control law (36) with $\widehat{\xi}$ satisfying (37) ensures that $e_{2w}(t)$ goes to zero in finite time, and $e_{2v}(t)$ goes to zero exponentially after $e_{2w}(t)$ reaches zero.

Proof: Details are available upon request.

IV. Stage 3: Orientation Error Correction

The orientation error will be regulated in this stage when there is no translation error. That is, when the robot reaches the desired position, the matrix $\boldsymbol{G}$ becomes

$$\boldsymbol{G}({}^{c}t_{*_x}, {}^{c}t_{*_z} = 0) = \begin{bmatrix} c\theta & 0 & f_u s\theta \\ 0 & 1 & 0 \\ -s\theta/f_u & 0 & c\theta \end{bmatrix}. \tag{38}$$

Thus the angular error signal in this stage can be selected as

$$e_3 \triangleq G({}^{c}t_{*_x}\, {}^{c}t_{*_z} = 0)_{13} \tag{39}$$

where the symbol $G({}^{c}t_{*_x}, {}^{c}t_{*_z} = 0)_{ij}$ denotes the element locating at i th row, j th column of $\boldsymbol{G}$ when both ${}^{c}t_{*_x} = 0$ and ${}^{c}t_{*_z} = 0$. It is easy to know that the robot points to the desired orientation when $e_3(t)$ goes to zero.

The open-loop dynamics is obtained after taking the time derivative of (39):

$$\dot{e}_3 = f_u c\theta \bullet \dot{\theta}. \tag{40}$$

After substituting (6) into (40) and utilizing (38), we obtain:

$$\dot{e}_3 = f_u G({}^{c}t_{*_x}, {}^{c}t_{*_z} = 0)_{11} w_c. \tag{41}$$

The controller of this stage is designed as

$$v_c = 0, \quad w_c = -k_3 G({}^{c}t_{*_x}, {}^{c}t_{*_z} = 0)_{11} e_3 \tag{42}$$

where $k_3 \in \mathbb{R}^+$ is a control gain.

Theorem 3: The controller (42) makes the system error (39) go to zero with exponentially convergent rate.

Proof : Details are available upon request.

V. Simulation Results

In this part, simulation results are provided to validate the proposed strategy. In the simulation, six static non-planar feature points are used to estimate $\boldsymbol{F}_S^{*c}$, in which three points are utilized to estimate $\boldsymbol{G}$. The intrinsic parameters of the virtual camera are set as:

$$f_u = 1003.7, f_v = 1006.3, u_0 = 376.9, v_0 = 285.3. \quad (43)$$

The initial pose of the robot is set as

$$(-6.1\mathrm{m}, 2.5\mathrm{m}, 3.0^\circ) \quad (44)$$

and the desired pose is $(0\mathrm{m}, 0\mathrm{m}, 0^\circ)$. The standard deviation of image noise is set as $\sigma = 0.15$ pixels.

As illustrated in section III, the system will find the configuration of pointing to the target position before stage 1. Thus the robot velocities are set as $v_c = 0,\ w_c = 0.01\mathrm{rad/s}$. Then $F_{S21\min}^{*c}$ can be obtained. After this process, $\theta(t)$ becomes 31.6°. Thus the pose of the robot before stage 1 becomes $(-6.1\mathrm{m}, 2.5\mathrm{m}, 31.6^\circ)$.

The controller gains and relative parameters are selected as

$$\begin{gathered} k_1 = 0.1, k_{2v} = 0.2, k_{2w} = 0.2, k_3 = 0.0001 \\ \widehat{\xi} = 1.3\xi, \kappa = 9, \eta = 11. \end{gathered} \quad (45)$$

The resultant path of the robot is shown in Fig. 4, it can be seen that the system behaves correctly despite the existence of the noise. It can be seen clearly that, the robot acts a pure rotation in stage 1 to point to the goal, and it then moves in a straight line mode to reach the desired position, finally it rotates to the desired orientation in the last stage.

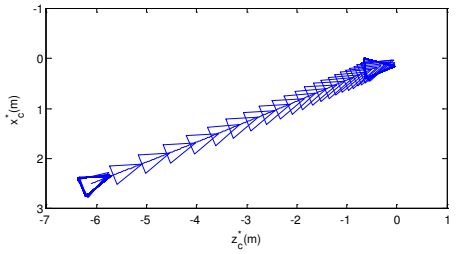

Fig. 4. Robot path

VI. Conclusion

For a nonholonomic mobile robot system equipped with an uncalibrated onboard camera, we propose a new method to address the visual servo regulation problem. Firstly, a fundamental matrix is used to control the orientation of the robot until it points toward the desired position, while the camera intrinsic parameters are estimated by using the fundamental matrix and a projection homography matrix. Subsequently, a straight-line motion controller is designed to drive the robot to the desired position and keep the robot pointing to the goal simultaneously. Finally, a pure rotation controller is used to correct the orientation error. The exponentially convergent properties of the error signals are proven with rigorous mathematical analysis. The performance of the proposed uncalibrated visual servoing strategy is validated by simulation results. Future efforts will target to utilize a pan mechanism to keep feature points visible during the serving process, and extend this strategy to some other platforms such as unmanned aerial robots.

References

[1] X. Zhang, Y. Fang, and X. Liu, "Motion-estimation-based visual servoing of nonholonomic mobile robots," *IEEE Trans. Robot.*, vol. 27, no. 6, pp. 1167-1175, Dec. 2011.

[2] D. Fontanelli, A. Danesi, F. A. W. Belo, P. Salaris, A. Bicchi, "Visual servoing in the large," *Int. J. Robot. Res.*, vol. 28, no. 6, pp. 802-814, 2009.

[3] G. Lopez-Nicolas, N. R. Gans, S. Bhattacharya, C. Sagues, J. J. Guerrero, and S. Hutchinson, "Homography-based control scheme for mobile robots with nonholonomic and field-of-view constraints," *IEEE Trans. Syst. Man Cybern. Part B-Cybern.*, vol. 40, no. 4, pp. 1115-1127, Aug. 2010.

[4] Y. Fang, X, Liu, and X. Zhang, "Adaptive active visual servoing of nonholonomic mobile robots," *IEEE Trans. Ind. Electron.*, vol. 59, no. 1, pp. 486-497, Jan. 2012.

[5] P. Murrieri, D. Fontanelli, and A. Bicchi, "A hybrid-control approach to the parking problem of a wheeled vehicle using limited view-angle visual feedback," *Int. J, Robot. Res.,* vol. 23, no. 4-5, pp. 437-448, 2004.

[6] R. T. Fomena, O. Tahri, F. Chaumette, "Distance-based and orientation-based visual servoing from three points," *IEEE Trans. Robot.*, vol. 27, no. 2, pp. 256-267, 2011.

[7] Z. Wang, D. -J. Kim, and A. Behal, "Design of stable visual servoing under sensor and actuator constraints via a Lyapunov-based approach," *IEEE Trans. Control Syst. Technol.*, vol. 20, no. 6, pp. 1575-1582, Nov. 2012.

[8] H. Hadj-Abdelkaker, Y. Mezouar, P. Martinet, and F. Chaumette, "Catadioptric visual servoing form 3D straight line," *IEEE Trans. Robot.*, vol. 24, no. 3, pp. 652-664, Jun. 2008.

[9] G. Oriolo, D. A. Luca, and M. Vendittelli, "WMR via dynamic feedback linearization: Design, implementation, and experimental validation," *IEEE Trans. Control Syst. Technol.,* vol. 10, no. 6, pp. 835-852, Nov. 2002.

[10] F. Chaumette and S. Hutchinson, "Visual servo control Part II: advanced approaches," *IEEE Robot. Autom. Mag.,* vol. 14, no. 2, pp. 109–118, Mar. 2007.

[11] E. Malis, F. Chaumette, and S. Bodet, "2 1/2 D visual servoing," *IEEE Trans. Robot. Autom.*, vol. 15, no. 2, pp. 238-250, Apr. 1999.

[12] G. Hu, W. MacKunis, N. Gans, et al., "Homography-based visual servo control with imperfect camera calibration," *IEEE Trans. Autom. Control*, vol. 54, no. 6, pp. 1318-1324, Jun. 2009.

[13] Y. –H. Liu, H. Wang, C. Wang, and K. K. Lam, "Uncalibrated visual servoing of robots using a depth-independent interaction matrix," *IEEE Trans. Robot.*, vol. 22, no. 4, pp. 804-817, Aug. 2006.

[14] A. Shademan and M. Jagersand, "Three-view uncalibrated visual servoing," *IEEE/RSJ Int. Conf. Intell. Robot. Syst.*, Oct. 2010, pp. 6234-6239.

[15] J. Piepmeier, G. M. Murray, and H. Lipkin, "Uncalibrated dynamic visual servoing," *IEEE Trans. Robot. Automat.*, vol. 20, no. 1, pp. 143–147, Feb. 2004.

[16] W. E. Dixon, D. M. Dawson, E. Zergeroglu, and A. Behal, "Adaptive tracking control of a wheeled mobile robot via an uncalibrated camera system," *IEEE Trans. Syst. Man Cybern. Part B-Cybern.*, vol. 31, no. 3, pp. 341–352, Jun. 2001.

[17] C. Wang, Z. Liang and Y. Liu, "Dynamic Feedback Robust Regulation of Nonholonomic Mobile Robots," in *Proc. IEEE Int. Conf. Decision and Control*, 2009, pp. 4384-4389.

[18] R. Hartley, A. Zisserman, *Multiple view geometry in computer vision (2nd ed.)*, UK: Camb. Univ. Press, 2003.

[19] G. L. Mariottini, G. Oriolo, and D. Prattichizzo, "Image-based visual servoing for nonholonomic mobile robots using epipolar geometry," *IEEE Trans. Robot.*, vol. 23, no. 1, pp. 87–100, Feb. 2007.